J. Phys. Chem. Solids Vol 41, pp 1119–1126
Pergamon Press Ltd., 1980. Printed in Great Britain

X-BAND ESR STUDIES OF FORBIDDEN TRANSITIONS OF EUROPIUM IONS IN CaF_2: Eu CRYSTALS

RYOHEI NAKATA, KATSUYASU KAWANO and MINORU SUMITA
University of Electro-Communications, Chofu-shi, Tokyo, Japan

and

EIICHI HIGUCHI
Tokyo Institute of Polytechnics, Nakano-ku, Tokyo Japan

(*Received* 17 *October* 1979; *accepted* 21 *March* 1980)

Abstract—The characteristics of allowed and forbidden transitions of Eu^{2+} ions in CaF_2 single crystals have been investigated at room temperature. The Angular dependences of these transition intensities were theoretically calculated with the use of perturbation theory, and compared with the experimental values. The experimental results can be explained by taking into account crystal field effects (1/60) b_4 $[O_4^0 + 5O_4^4]$, and a hyper fine interaction $A_i\mathbf{S}\cdot\mathbf{I}_i$ in the spin Hamiltonian.

INTRODUCTION

ESR and ENDOR studies of Eu^{2+} ions in a cubic crystal field in CaF_2 crystals have been made by many authors[1–5]. In addition to prominent spectra corresponding to well known allowed transitions, several spectra corresponding to forbidden transitions have been observed. Lee *et al.* observed the forbidden transition spectra, $\Delta M = \pm 2$ through ± 7 and $\Delta m = 0$, by using an X-band ESR spectrometer[3], while Bleaney *et al.* comment briefly on other forbidden transition spectra, $\Delta M = \pm 1$ and $\Delta m \neq 0$[6]. Re-examinations of these results have been carried out based upon the experimental analyses described below.

Investigations of the oxidation and reduction of europium ions in CaF_2 require detailed information on both allowed and forbidden transition spectra, since foreign impurities such as OH^- and/or O^{2-} ions are introduced in the lattice through the oxidation process, and result in modification of the cubic crystal field around the europium ions. For example, Eu^{2+} ions in a cubic crystal field are oxided to Eu^{3+} ions under heat-treatment in a hydrolyzing atmosphere at high temperatures, and reduction to Eu^{2+} ions under X-ray irradiation takes place at room temperature[4]. Hence the environment around the reduced Eu^{2+} ions might not be the same as for Eu^{2+} ions as-grown CaF_2. Another reason is that the prominent hyperfine forbidden spectra found in each fine spectrum are difficult to identify, and the angular dependences of forbidden hyperfine line intensities deviate markedly from the calculated results[7]. As a result, better determined allowed and forbidden transition intensities need to be derived for a center with a large cubic crystal field parameter, b_4, as in the present case, for comparison with the experimental results.

THEORETICAL

The spin Hamiltonian of Eu^{2+} ions in a cubic field is given by

$$\mathcal{H} = g\beta\,\mathbf{H}\cdot\mathbf{S} + (1/60)b_4[O_4^0 + 5O_4^4] + (1/1260)b_6[O_6^0 - 21O_6^4] + A_i\mathbf{S}\cdot\mathbf{I}_i \quad (1)$$

where $S = 7/2$, $I_i = 5/2$, and A_i are the hyperfine constants of ^{151}Eu and ^{153}Eu respectively. The spin Hamiltonian parameters reported so far are listed in Table 1. Both theoretical and experimental investigations of the forbidden transition probability has been performed in iron group ions by taking into account the effects of the second and last terms in eqn (1)[6–8], but little is known about the rare earth ions. Following Bleaney's procedure[6], a perturbation calculation to derive the forbideen transition probability has been performed in the present study by considering the effects of the cubic crystal and hyper fine structure (h.f.s.) terms in eqn (1). The S_z axis in eqn (1) was transformed from the crystal axis to the external magnetic field direction, and the angular dependence of the transition probability was calculated in the latter co-ordinate system. As we are

Table 1. Spin Hamiltonian parameters after Baker and Williams*

g	= 1.9926
b_4	= −63.13 (G)
b_6	= +0.28 (G)
A_{151}	= −36.89 (G)
A_{153}	= −16.37 (G)

*Reference 5.

principally interested in the forbidden transitions associated with the nuclear spin flipping, the spin Hamiltonian is given approximately after operating on a basis spin state $[M, m)$ on the right side by

$$\begin{aligned}\mathcal{H}[M,m) \fallingdotseq\ & g\beta HM[M,m) \\ & + (1/60)b_4\{F(\theta,\phi)f_+(M)S_+^2[M,m) \\ & + G(\theta,\phi)g_+(M)S_+[M,m) + J(\theta,\phi)j(M)[M,m) \\ & + G^*(\theta,\phi)g_-(M)S_-[M,m) \\ & + F^*(\theta,\phi)f_-(M)S_-^2[M,m)\} \\ & + (1/1260)b_6\{Q(\theta,\phi)q_+(M)S_+(M)[M,m) \\ & + R(\theta,\phi)r(M)[M,m) \\ & + Q^*(\theta,\phi)q_-(M)S_-[M,m)\} + A_iS\cdot I_i[M,m)\end{aligned} \tag{2}$$

where

$$\begin{aligned}F(\theta,\phi) &= (5/4)\sin^2\theta[7\cos^2\theta - 1 + (\cos^2\theta + 1)\cos 4\phi \\ &\quad + i2\sin 4\phi \sin^2\theta] \\ G(\theta,\phi) &= -(5/4)\sin\theta[\cos\theta(7\cos^2\theta - 3) \\ &\quad -\cos\theta\sin^2\theta\cos 4\phi - i\sin 4\phi\sin^2\theta] \\ J(\theta,\phi) &= (1/8)[35\cos^4\theta - 30\cos^2\theta + 3 + 5\sin^4\theta\cos 4\phi] \\ Q(\theta,\phi) &= -(1/16)\sin\theta[\cos\theta(33\cos^4\theta - 30\cos^2\theta + 5) \\ &\quad + \sin^2\theta\cos\theta(33\cos^2\theta - 13)\cos 4\phi \\ &\quad + i2\sin^2\theta(11\cos^2\theta - 1)\sin 4\phi] \\ R(\theta,\phi) &= (1/16)[231\cos^6\theta - 315\cos^4\theta \\ &\quad + 105\cos^2\theta - 5 \\ &\quad - 21\sin^4\theta(11\cos^2\theta - 1)\cos 4\phi] \\ f_\pm(M) &= 7M^2 \pm 14M - S(S+1) + 9 \\ g_\pm(M) &= 14M^3 \pm 21M^2 - 6S(S+1)M \\ &\quad + 19M \mp 3S(S+1) \pm 6 \\ j(M) &= 35M^4 - 30S(S+1)M^2 + 25M^2 + 3S^2(S+1)^2 \\ &\quad - 6S(S+1) \\ q_\pm(M) &= 1386M^5 \pm 3465M^4 - 1260S(S+1)M^3 + 7560M^3 \\ &\quad \mp 1890S(S+1)M^2 \pm 7875M^2 + 210S^2(S+1)^2M \\ &\quad - 2310S(S+1)M + 4914M \pm 105S^2(S+1)^2 \\ &\quad \mp 840S(S+1) \pm 1260 \\ r(M) &= 231M^6 - 315S(S+1)M^4 + 735M^4 \\ &\quad + 105S^2(S+1)^2M^2 - 525S(S+1)M^2 \\ &\quad + 294M^2 - 5S^3(S+1)^3 \\ &\quad + 40S^2(S+1)^2 - 60S(S+1)\end{aligned} \tag{3}$$

$F^*(\theta,\phi)$, $G^*(\theta,\phi)$ and $Q^*(\theta,\phi)$ are the complex conjugates of $F(\theta,\phi)$, $G(\theta,\phi)$ and $Q(\theta,\phi)$, respectively, and the $S_\pm^2$ terms arising from $[O_6^6 - 21O_6^4]$ are omitted because their contribution is negligible. Using eqns (2) and (3), we can calculate spin wave functions mixed mutually through $S_\pm^2$, $S_\pm$ and $A_i\mathbf{S}\cdot\mathbf{I}_i$. From second order perturbation theory, the spin wave function $\Psi(M,m)$ is derived as follows.

$$H_o = (h\nu/g\beta) \gg |b_4| \text{ and } |b_6| \tag{4}$$

$$\begin{aligned}\Psi(M,m) = N(M,m)\{&[M,m) + (A_i/2H_o) \\ &\times\sqrt{[(S+M)(S-M+1)(I_i-m)(I_i+m+1)]} \\ &\times[M-1,m+1) - (A_i/2H_o) \\ &\times\sqrt{[(S-M)(S+M+1)(I_i+m)(I_i-m+1)]} \\ &\times[M+1,m-1)' - (b_4/60MH_o)G(\theta,\phi)j(M) \\ &\times\sqrt{[(I_i-m)(I_i+m+1)]}\,[M,m+1) \\ &+ (b_4/60MH_o)G^*(\theta,\phi)j(M) \\ &\times\sqrt{[(I_i+m)(I_i-m+1)]}\,[M,m-1) \\ &-(A_ib_4/160MH_o^2)F(\theta,\phi)j(M) \\ &\times\sqrt{[(I_i-m)(I_i+m+1)(I_i-m-1)(I_i+m+2)]}\,[M,m+2) \\ &+(A_ib_4/160MH_o^2)F^*(\theta,\phi)j(M) \\ &\times\sqrt{[(I_i+m)(I_i-m+1)(I_i+m-1)(I_i-m+2)]}\,[M,m-2) \\ &-(b_6/60MH_o)Q(\theta,\phi)r(M) \\ &\times\sqrt{[(I_i-m)(I_i+m+1)]}\,[M,m+1) \\ &+(b_6/60MH_o)Q^*(\theta,\phi)r(M) \\ &\sqrt{[(I_i+m)(I_i-m+1)]}\,[M,m-1)\}\end{aligned} \tag{5}$$

where $N(M,m)$ is a normalization constant and is given by

$$\begin{aligned}N^{-1}(M,m) = \{&1 + 2([b_4j(M)/60MH_o]^2G(\theta,\phi)G^*(\theta,\phi) \\ &+ [b_6r(M)/60MH_o]^2Q(\theta,\phi)Q^*(\theta,\phi)) \\ &\times[I_i(I_i+1) - m^2] \\ &+ 2[A_ib_4j(M)/160MH_o^2]^2F(\theta,\phi)F^*(\theta,\phi) \\ &\times[m^4 - 2I_i(I_i+1)m^2 + 5m^2 \\ &+ (I_i-1)I_i(I_i+1)(I_i+2)]\}^{1/2}\end{aligned} \tag{6}$$

$$\begin{aligned}\fallingdotseq\{&1 + 2[b_4j(M)/60MH_o)]^2G(\theta,\phi)G^*(\theta,\phi) \\ &\times[I_i(I_i+1) - m^2]\}^{1/2}.\end{aligned} \tag{6'}$$

The corresponding energy $E(M,m)$ is also derived approximately

$$\begin{aligned}E(M,m) = &\ g\beta HM + (b_4/60)j(M)J(\theta|\phi) \\ &+ (b_6/1260)r(M)R(\theta,\phi) + A_iMm \\ &+ (A_i^2/2H_o)[M^2 - S(S+1)]m \\ &- (A_i^2-2H_o)M(m^2 - I_i(I_i+1)] \\ &+ (2A_i/H_o^2)(b_4/60M)j(M)G(\theta,\phi) \\ &+ (b_6/1260)r(M)R(\theta,\phi)|^2Mm.\end{aligned} \tag{7}$$

The transition probability $P(M,m\to M+1,n)$ can be calculated by the usual formula

$$\begin{aligned}P(M,m\to M+1,n) \propto [N(M,m)N(M+1,n)]^2\Big|\int\Psi^*(M \\ +1,n)S_j\Psi(M,m)d\tau\Big|^2\end{aligned} \tag{8}$$

where S_j is the polarization of the microwave magnetic field. When a cylindrical TE_{011} cavity is used, S_j in eqn (8) can be replaced by S_+ in good approximation despite smaller contributions from S_-. Then the transition probabilities under consideration are as follows,

$$\begin{aligned}P(M,m\to M+1,m) \propto &\ [N(M,m)N(M+1,m]^2|1 \\ &+ a(M,m)a^*(M+1,m) \\ &+ a(M+1,-m)a^*(M,-m) \\ &+ b(M,m)b^*(M+1,m) \\ &+ b(M+1,-m)b^*(M,-m)|^2(S-M)(S+M+1)\end{aligned}$$

$$\begin{aligned}&P(M,m\to M+1,m\pm1) \\ &\quad\propto [N(M,m)N(M+1,m\pm1)]^2|a(M,\pm m) \\ &\quad - a(M+1,\mp m-1) \\ &\quad \pm a^*(M,\mp m)b(M+1,\mp m-1) \\ &\quad \pm a(M+1,\pm m+1)b^*(M\pm m)|^2(S-M)(S+M \\ &\quad +1)\end{aligned}$$

$$P(M,m\rightarrow M+1,m\pm2) \propto [N(M,m)N(M+1,m\pm2)]^2|b(M,\pm m) - b(M+1,\mp m-2) \mp a(M,\pm m)a(M+1,\mp m-2)|^2(S-M)(S+M+1) \quad (9)$$

where

$$a(M,m=-(1/60MH_o) \times[b_4G(\theta,\phi)j(M)+b_6Q(\theta,\phi)r(M)] \times[(I_i-m)(I_i+m+1)]^{1/2}$$

$$b(M,m)=(A_ib_4/160MH_o^2)F(\theta,\phi)j(M) \times[(I_i-m)(I_i+m+1)(I_i-m-1)(I_i+m+2)]^{1/2} \quad (10)$$

and $a^*(M,m)$ and $b^*(M,m)$ are the complex conjugates of $a(M,m)$ and $b(M,m)$, respectively. The crystal field parameter $|b_4|$ is much larger than $|b_6|$ in the present case as listed in Table 1, and hence b_6 contributes only a few percent at the most to the transition probabilities. Some of the numerical results are shown in Figs. 1 and 2, where the external magnetic field was rotated in the $(1\bar{1}0)$ plane ($\phi=45°$). In addition to these transitions, similar procedures were applied to the calculation of the forbidden transition probabilities of low magnetic field spectra. The transition probabilities for $\Delta M=2$ with $\Delta m=0$ and ±1 are given by

$$P(M,m\rightarrow M+2,m) \propto [N(M,m)N(M+2,m)]^2(b_4/60)^2(S-M)(S+M+1)(S-M-1)(S+M+2) \times\{g_+(M)/[E(M)-E(M+1)] + g_-(M+2)/[E(M+2)-E(M+1)] - (A_i/4)((I_i+m) \times(I_i-m+1)/[(M+2)E(M) - (M+2)E(M+1)])(k_-(M+2)/[E(M+2) - E(M+1)] + k_-(M+3)/[E(M+2)-E(M+3)]) + (A_i/4)((I_i-m) \times(I_i+m+1)/[ME(M+2) - ME(M+1)]) \times(k_+(M)/[E(M)-E(M+1)] + k_+(M-1)/[E(M) - E(M-1)])\}^2G(\theta,\phi)G^*(\theta,\phi)$$

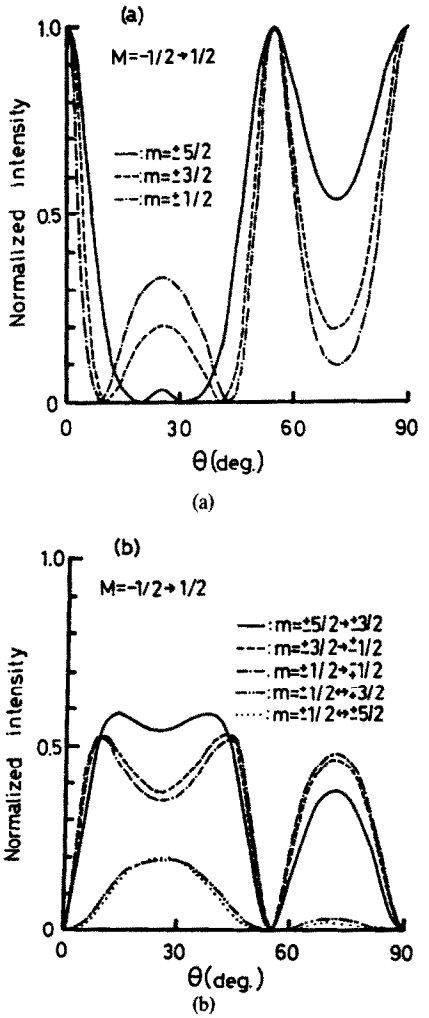

Fig. 1. Calculated angular dependences for $M=-1/2\rightarrow+1/2$, (a) allowed and (b) forbidden transitions, respectively.

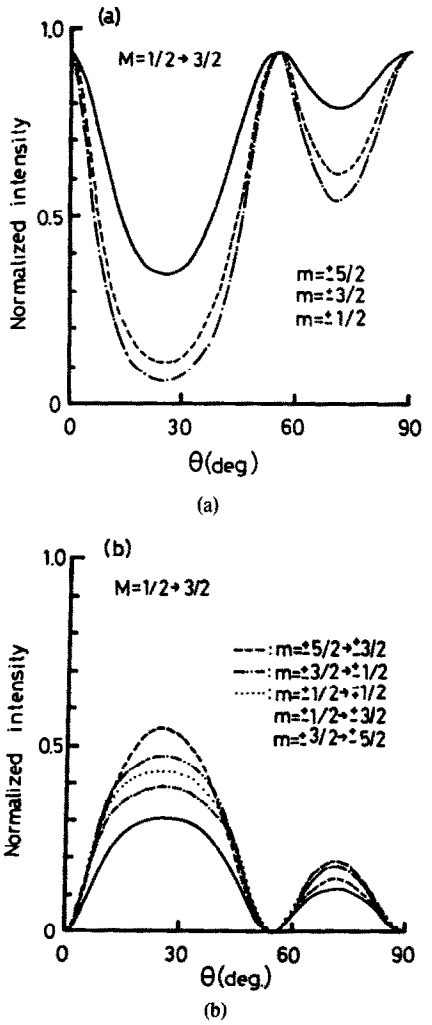

Fig. 2. Calculated angular dependences for $M=1/2\rightarrow3/2$, (a) allowed and (b) forbidden transitions, respectively.

$$P(M,m\to M+2,m+1)$$
$$\propto [N(M,m)N(M+2,m+1)]^2(b_4/120)^2(S-M)(S+M+1)(S-M-1)(S+M+2)(I_i-m)(I_i+m+1)\{(g_+(M)/[(M+2)E(M)-(M+2)E(M+1)])(k_-(M+2)/[E(M+2)-E(M+1)]+k_-(M+3)/[E(M+2)-E(M+3)])-(g_-(M+2)/[ME(M+2)-ME(M+1)])\times(k_+(M)/[E(M)-E(M+1)]+k_+(M-1)/[E(M)-E(M-1)])\}^2[G(\theta,\phi)G^*(\theta,\phi)]^2$$

$$P(M,m\to M+2,m-1)$$
$$\propto [N(M,m)N(M+2,m-1)]^2[(S-M)(S+M+1)(S-M-1)(S+M+2)(I_i+m)(I_i-m+1)]\Big\{(A_i/2)(1/[E(M+2)-E(M+1)]+1/[E(M)-E(M+1)])+(b_4/120)^2\{(g_-(M+2)/[ME(M+2)-ME(M+1)])\times(k_-(M)/[E(M)-E(M-1)]+k_-(M+1)/[E(M)-E(M+1)])-(g_+(M)/[(M+2)E(M)-(M+2)E(M+1)])\times(k_+(M+1)/[E(M+2)-E(M+1)]+k_+(M+2)/[E(M+2)-E(M+3)]\}G(\theta,\phi)G^*(\theta,\phi)\Big\}^2 \quad (11)$$

where $k_\pm(M)=14M^5\pm35M^4+40M^3-20S(S+1)M^3\pm25M^2\mp30S(S+1)M^2+6M-22S(S+1)M+6S^2(S+1)^2M\pm3S^2(S+1)^2\mp6S(S+1)$

$$E(M)\doteqdot g\beta HM+(b_4/60)J(\theta,\phi)j(M)+(b_6/1260)R(\theta,\phi)r(M). \quad (12)$$

It is clear that $P(M,m\to M+2,m)$ and $P(M,m\to M+2,m+1)$ become zero at $\theta=0$, 54.7 and 90, while $P(M,m\to M+2,m-1)$ does not become zero at these angles. In the latter case

$$P(M,m\to M+2,m-1)\propto [(S-M)(S+M+1)(S-M-1)(S+M+2)(I_i+m)(I_i-m+1)](A_i/2)^2\{[E(M+2)-E(M+1)]^{-1}+[E(M)-E(M+1)]^{-1}\}^2 \quad (13)$$

Table 2. Normalized transition intensities and fine structure line positions of $(M,m)\to(M+2,m-1)$ transitions at $\theta=0$, 54.7 and 90°

1) $\theta = 0^\circ$

M	m = 1/2	m = -1/2,3/2	m = -3/2,5/2	H(G)
-7/2	0.0144	0.0128	0.0080	1382
-5/2	0.0000	0.0000	0.0000	2361
-3/2	0.0035	0.0031	0.0020	2079
-1/2	0.0035	0.0031	0.0020	1318
1/2	0.0000	0.0000	0.0000	1036
3/2	0.0144	0.0128	0.0080	2015

2) $\theta = 54.7^\circ$

M	m = 1/2	m = -1/2,3/2	m = -3/2,5/2	H(G)
-7/2	0.0042	0.0038	0.0024	1907*
-5/2	0.0000	0.0000	0.0000	1257
-3/2	0.0014	0.0013	0.0008	1450*
-1/2	0.0014	0.0013	0.0008	1948*
1/2	0.0000	0.0000	0.0000	2140
3/2	0.0042	0.0038	0.0024	1490*

3) $\theta = 90^\circ$

M	m = 1/2	m = -1/2,3/2	m = -3/2,5/2	H(G)
-7/2	0.00043	0.00038	0.00024	1779
-5/2	0.00001	0.00001	0.00000	1533
-3/2	0.00021	0.00019	0.00012	1601
-1/2	0.00021	0.00019	0.00012	1796
1/2	0.00001	0.00001	0.00000	1864
3/2	0.00043	0.00038	0.00024	1618

* (M,m) → (M+2,m-1) and (M,m) → (M+2,m) transitions overlap. The latter transitions are caused by mixing of cubic crystal fields in eqn (1)

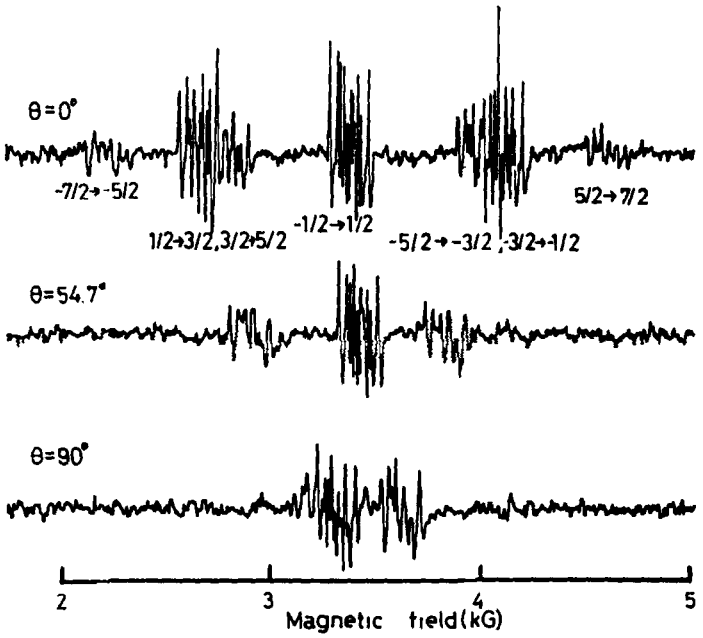

Fig. 3. ESR spectra of Eu^{2+} ions in three directions.

and the resonance condition is

$$E(M+2) - E(M) = H_o. \tag{14}$$

Transition intensities (probabilities normalized by the allowed transition probability of $M = -1/2 \rightarrow +1/2$ at $\theta = 0°$) and fine structure line positions were calculated and are listed in Table 2.

EXPERIMENTAL PROCEDURE AND RESULTS

CaF_2:Eu crystals were grown *in vacuo* by the Stockbarger method. Europium chloride ($EuCl_3 \cdot 6H_2O$) powder and crushed CaF_2 crystals, which were optically pure and obtained from Oyokoken Kogyo Ltd., were placed in a carbon crucible in a vacuum furnace. Before melting the mixture, care was taken to remove adsorbed water vapor and water of crystallization from $EuCl_2 \cdot 6H_2O$ *in vacuo* below 300°C. ESR measurements were performed at room temperature with a conventional X-band spectrometer with a frequency-stabilized Gunn oscillator and 100 kHz magnetic field modulation.

Typical ESR spectra are shown in Fig. 3. Figure 4 shows a part of the spectra corresponding to the transition, $M = -1/2 \rightarrow +1/2$, $\Delta m = 0$ and ± 1. At $\theta = 0°$, hyperfine structure (h.f.s.) lines of the allowed transition spectra have the largest intensity, and only traces of the forbidden transition spectra may be expected to appear in the middle of the h.f.s. lines for the allowed transitions. On the other hand, the former h.f.s. lines decrease considerably and the latter increase remarkably at $\theta = 15°$. Similar results are shown in Fig. 5 for $M = 1/2 \rightarrow 3/2$ together with $M = -1/2 \rightarrow +1/2$ transitions. Figure 6 shows the angular dependences of the normalized intensities of both the allowed and the forbidden ($\Delta m = \pm 1$) h.f.s. lines between the $M = -1/2$ and $+1/2$ transition. The open circles and squares represent experimental results for the forbidden and allowed transitions, respectively, while the solid lines represent the theoretical ones. The experimental results coincide fairly well with the theoretical ones. Deviations of the experimental results from the calculated line for $\Delta m = \pm 1$ in the region above $\theta = 10°$ are due to overlap of the forbidden h.f.s. doublet lines as shown in Fig. 4. Figure 7 shows the behavior of the h.f.s. spectra for $M = -1/2 \rightarrow +1/2$ around $\theta = 55°$. As the theoretical calculation showed, the intensities of the forbidden transition spectra fall to zero at $\theta = 54.7°$, the[11] direction, and again rise with further angular variation. In the low magnetic field region we found several weak spectra corresponding to the forbidden transitions, $\Delta M = 2$, and some of these are shown in Fig. 8, where the magnetic field lies along one of the three crystallographic axes ($\theta = 0$, 54.7 and 90°). Since the transition probabilities $P(M,m \rightarrow M +$

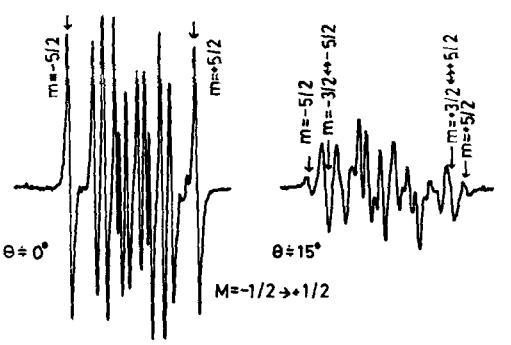

Fig. 4. Variations of allowed and forbidden transitions for two directions under the same measuring conditions.

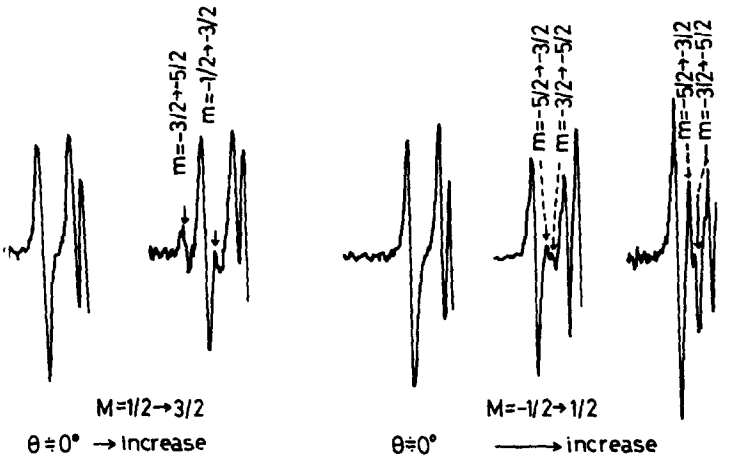

Fig. 5. Allowed and forbidden transitions near $\theta = 0°$ in the $(1\bar{1}0)$ plane.

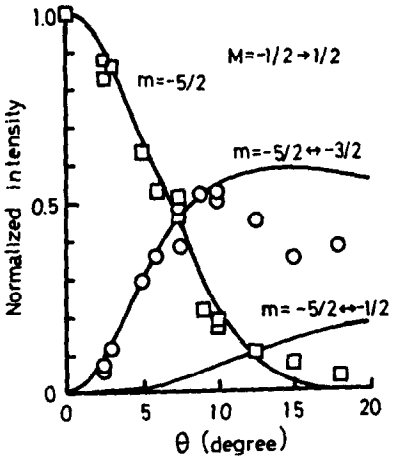

Fig. 6. Angular variations of transition intensities. Squares and circles are experimental results for allowed and forbidden transitions, respectively, and solid lines are calculated from eqn (10) when $b_6 = 0$.

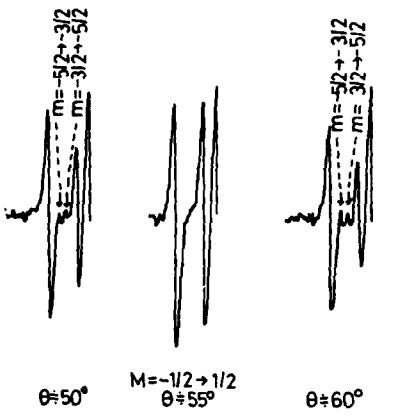

Fig. 7. Allowed and forbidden transitions near $\theta = 55°$.

$2, m-1$) are not zero at these three angles as indicated by eqn (13), the unknown spectra were assigned as shown in Fig. 8 with the aid of their fine structure (fs) line positions in Table 2.

Besides the allowed and forbidden transition probabilities, the angular dependence of the effective h.f.s. constant is of interest. From eqn (7), the effective h.f.s. constant for the state M is given approximately by

$$A_{i\text{eff}}(M) \doteqdot A_i[1 + 2(b_4/60M)^2 j^2((M)G(\theta,\phi)G^*(\theta,\phi)]. \quad (15)$$

Using this equation, the separations between two allowed outer h.f.s lines were calculated, and are given by

$$5A_i[1 + 648(b_4/60H_o)^2 G(\theta,\phi)G^*(\theta,\phi)] \quad \text{for } M = -1/2 \rightarrow +1/2 \quad (16)$$

and

$$5A_i[1 - 312(b_4/60H_o)^2 G(\theta,\phi)G^*(\theta,\phi)] \text{ for } M = 1/2 \rightarrow 3/2. \quad (17)$$

The calculated and experimental results are shown in Fig. 9 for eqn (16), where the complicated f.s. and h.f.s. spectra make it difficult to compare these results over all the magnetic directions in the $(1\bar{1}0)$ plane. The latter angular dependences could not be analyzed because the h.f.s. lines arising from the $M = 1/2 \rightarrow 3/2$ and $3/2 \rightarrow 5/2$ transitions overlap one another around 3 kG as shown in Fig. 3.

DISCUSSION

We have derived formal expressions for the allowed and forbidden transition probabilities based on perturbation theory, and compared them with the experimental results to confirm the forbidden transition spectra. The agreement between the theoretical and experimental results is very good.

It is clear from the perturbation treatment that the

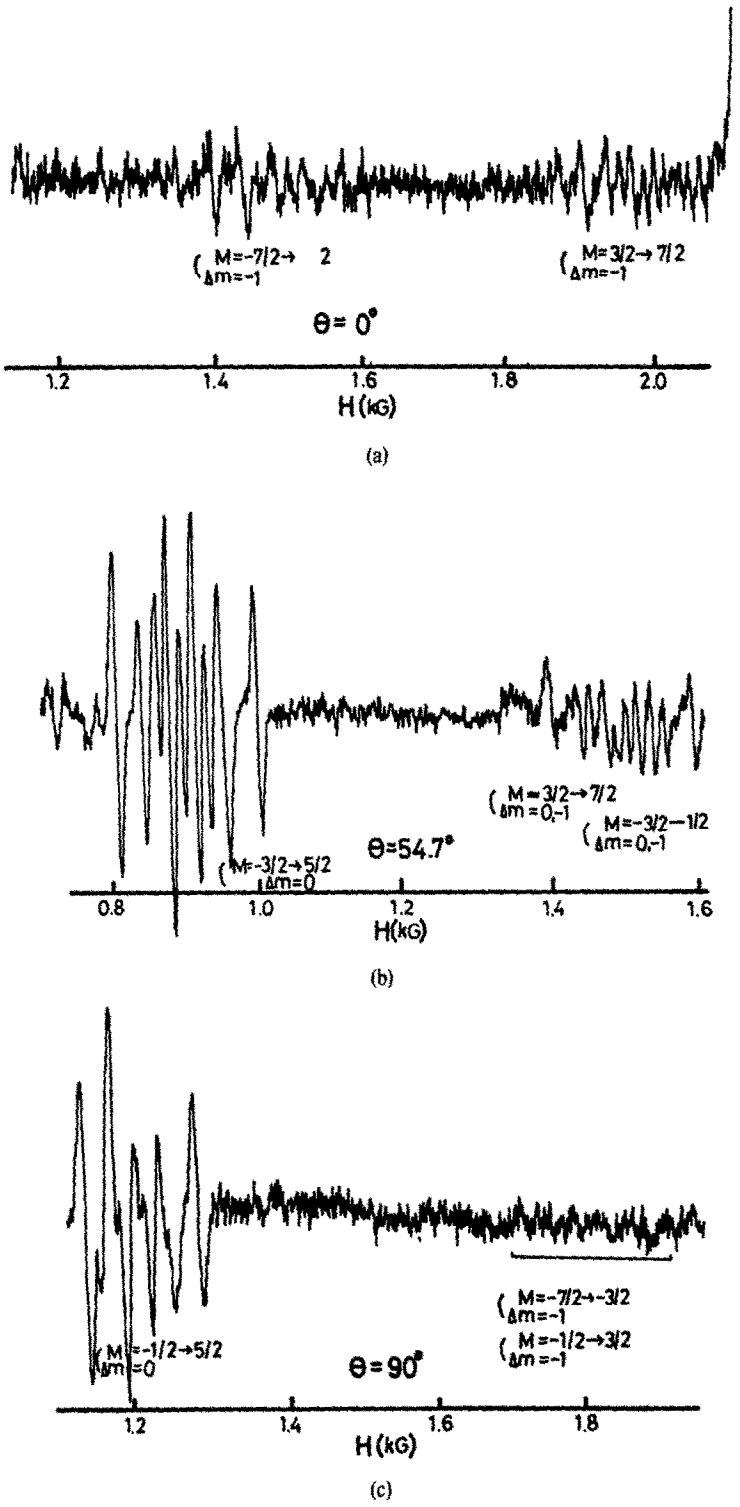

Fig. 8. Low magnetic field ESR spectra, (a) $\theta = 0°$, (b) 54.7° and (c) 90°, respectively. Types of transitions are indicated for each set of spectra.

transition probabilities (or line intensities) depend on the relative values of the crystal field and h.f.s. terms to the Zeeman term in eqn (1). As shown in Fig. 1(a), the dissappearance of the allowed h.f.s. lines occurs at different angles, which are dependent on the microwave frequency utilized. Table 3 shows results for the maximum ESR frequency needed for observing the dissappearance of the allowed h.f.s. lines ($M = -1/2 \rightarrow +1/2$ and $\Delta m = 0$) in various crystals, in which the dominant crystal field parameters b_4 are shown in the right column.

Table 3. Calculated maximum ESR frequency needed for observing the complete disappearance of the allowed $M = -1/2 \rightarrow +1/2$ transition in various crystals

crystals	m = ±1/2	m = ±3/2	m = ±5/2	$\|b_4\|$ (G)
CaF_2	18334 (MHz)	16032 (MHz)	9942 (MHz)	63.13 a)
SrF_2	13950	12199	7564	48.06 b)
BaF_2	10955	9615	5965	37.88 c)
$SrCl_2$	4058	3550	2201	13.96 d)
CaO	8024	7017	4353	27.65 e)

a): reference 5), b):9), c):10), d):11) and e):12), respectively.

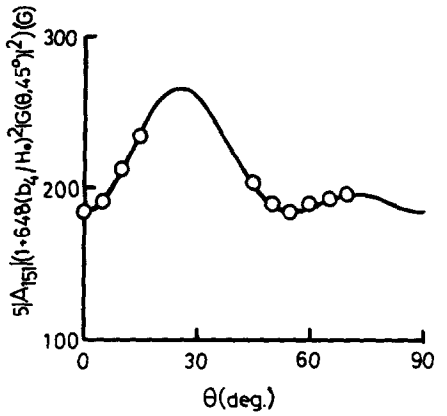

Fig. 9. Separation of outer two h.f.s. lines for $M = -1/2 \rightarrow +1/2$ transition. Circles are experimental results and the solid line is calculated from eqn (14).

Table 3 indicates that Eu^{2+} ions in fluorite structures such as SrF_2 and BaF_2 are also suitable and interesting ions for investigating allowed and forbidden transitions at X-band frequencies from theoretical and experimental points of view; that is, the ratios (b_4/H_o) are of the proper order for observing this behavior. However, the complete dissappearance of the allowed h.f.s. lines could not be confirmed in our experiments, because the allowed $m = \pm 1/2$ and $\pm 3/2$ h.f.s. lines were masked by overlapping of various h.f.s. lines due to Eu^{151} and Eu^{153}, while the $m = \mp 5/2$ lines were also masked above $\theta = 20°$ by the allowed h.f.s. lines due to the $M = \pm 5/2 \leftrightarrows \pm 3/2$ transitions. Figure 5 shows that the allowed h.f.s. lines ($M = 1/2 \rightarrow 3/2$ and $m = -5/2$) decrease with increasing θ from $\theta = 0°$, while the forbidden transition ($M = 1/2 \rightarrow 3/2$ and $m = -3/2 \rightarrow -5/2$) increases. This angular behavior coincides well with the results shown in Figs. 2 and 3 below $\theta = 10°$. It is noted that the normalization constants in eqn (6) are taken into consideration in the present calculation.

The separation ΔH between the forbidden doublet h.f.s. lines for $M = -1/2 \rightarrow +1/2$, as shown in Fig. 5 by arrows, is calculated from eqn (7) and is

$$\Delta H = 31 A_i^2 / 2 H_o . \tag{18}$$

The numerical result is 6.2(*G*), which agrees with the experimental value ~6(*G*). This doublet structure is one of the characteristic features of the forbidden transition between the $M = -1/2$ and $+1/2$ states, and the separation should be independent of (θ, ϕ), as given in eqn (18). Similar doublet lines were observed for Mn^{2+} ions in ZnSe[7] and MgO[8], in which the spearations are much larger than that for Eu^{2+} ions CaF_2. It is, however, puzzling why the doublet lines in Fig. 4 overlap at $\theta = 15°$ with the same measurement conditions as at $\theta = 0°$.

The forbidden h.f.s. spectra observed at low magnetic field were assigned by both the transition probabilities and corresponding f.s. line positions. The former transition probabilities are strongly dependent on the polar angles (θ, ϕ) through

$$G(\theta,\phi)G^*(\theta,\phi) = (25/16)\sin^2\theta\{[\cos\theta(7\cos^2\theta - 3) - \cos 4\phi \cos\theta \sin^2\theta]^2 + [\sin 4\phi \sin^2\theta]^2\}. \tag{19}$$

The small mis-orientation of the crystal axes leads to all the transitions in eqn (11) being allowed, and causes mixing of the wave-functions through the cubic field terms in eqn (1), which also produce forbidden transitions. Although the ESR spectra were traced by adjusting θ and ϕ around the crystal (001) axis, we did not observe complete extinction of these non-identified h.f.s. spectra[3]. Accordingly, our assignments of these non-identified spectra are probably correct.

REFERENCES

1. Baker J. M., Bleaney B. and Hayes W., *Proc. Roy. Soc*, **A247**, 141 (1958).
2. Low W., *Phys. Rev.* **109**, 265 (1958).
3. Lee S., Menne T. J. and Paxhia E. C., *J. Chem. Phys.* **50**, 5129 (1969).
4. Nakata R., Kawano K., Sumita M., and Higuchi E., *J. Phys. Chem. Solids* **40**, 955 (1979).
5. Barker J. M. and Williams F.I.B., *Proc. Roy. Soc.* **A267**, 283 (1962).
6. Bleaney B. and Rubins R. S., *Proc. Phys. Soc. (London)* **77**, 103 (1962).
7. Cavenett B. C., *Proc. Phys. Soc.* **84**, 1 (1964).
8. Drumheller J. E. and Rubins R. S., *Phys. Rev.* **133**, A1099 (1964).
9. Title R. S., *Phys. Lett.* **6**, 13 (1963).
10. Hurren W. R., Nelson H. M., Larson E. G. and Gardner J. H., *Phys. Rev.* **185**, 624 (1969).
11. Low W. and Rosenberger U., *Phys. Rev.* **116**, 621 (1959).
12. Shuskus A. J., *Phys. Rev.* **127**, 2022 (1963).